Study of relative permeability curves for a CO_2-brine system at reservoir conditions in carbonates

Jorge Tovar[1,*], *Tatiana* Berna[1], *Tálisson* Borges[1], *Janeth* Vidal[2], *Rafael* Valladares[3], *Gabriel* Soares[3], and *Erika* Koroishi[2].

[1]University of Campinas - UNICAMP, Faculty of Mechanical Engineering, Rua Mendeleyev 200, Campinas, SP, Brazil
[2]Center for Petroleum Studies - CEPETRO, Miscible Methods of Recovery Laboratory - LMMR, Rua Cora Coralina 350, Campinas, SP, Brazil
[3]Repsol Sinopec Brazil S.A, Research and Development Department, Praia de Botafogo 300, Rio de Janeiro, RJ, Brazil

Abstract. This work presents an experimental study to determine unsteady-state drainage and imbibition relative permeability curves by coreflooding in a two-phase system: equilibrated carbonated brine (ECB) and supercritical CO_2 ($scCO_2$), using Brazilian Pre-salt carbonate rocks under reservoir conditions (8,500 psi and 70ºC). Saturation changes in the rock were monitored by computed tomography (CT) and mass balance. As analytic methods to build relative permeability curve such as Johnson, Bossler and Neuman (JBN) are not valid due to the confirmed presence of fingering, relative permeability curves were defined using the Corey model and Corey exponents found in literature related to this work. Results showed a slow increase of CO_2 relative permeability and a rapid decrease of ECB relative permeability during the first part of the drainage. Also, at the end of the drainage a residual ECB saturation of 27% was achieved. Furthermore, during the imbibition, the hysteresis effect was observed on the ECB relative permeability curve as a result of the CO_2 trapped (19.5%). In addition, evidence that the ECB is not strongly wetting the rock in the presence of CO_2 is presented. Finally, the Land trapping parameter was calculated along the composite core.

1 Introduction

The high CO_2 concentration of produced field gas in Brazilian Pre-Salt reservoirs (10 to 45%) brings essential technological challenges for the applicability of CO_2. For example, the separation of this gas is necessary before transferring to onshore facilities, because the transportation of high CO_2 content gas is not feasible due to its corrosive effects in transport facilities [1]. Nowadays, CO_2 separation equipment is expensive, high energy-consumer, and takes up a significant area of the floating production storage and offloading vessel (FPSO) [1]. On the other hand, flaring could be the most straightforward and cheapest option to dispose this gas. Nevertheless, regulations to control this practice are more rigid every time [2]. For the reasons explained above, it is necessary to find ways to use or store CO_2 to avoid negative impacts on the environment and damage to facilities.

Otherwise, the growing energy demand worldwide in the context of a low-carbon energy transition encourages CO_2 utilization for Enhanced Oil Recovery (EOR) solutions, which improves oil productivity while safely disposing of a gas that would contribute to global warming. As a consequence, CO_2-WAG (Water Alternating Gas) has been applied in Brazilian offshore oilfields to improve recovery rates and mitigate the environmental impact that venting CO_2 would bring [3].

The alternating injection of water and gas was conceived to compensate the counter tendencies of gas rising upward and water falling downward inside the reservoir by dividing the continuous slug of gas into smaller slugs by alternating water banks [4]. On the other hand, injecting water with miscible gas reduces the instability of the gas/oil displacement, improving the overall sweep efficiency [5].

Consequently, CO_2-WAG projects are sensitive to fluid-rock and fluid-fluid interactions, beyond the characterization of the rock and fluids themselves [5]. Hence, relative permeability curves and their associated parameters are the most relevant petrophysical relations for EOR processes [6]. That is why understanding the physics behind which CO_2 and water displacing oil in the porous medium is of utmost importance for the success of any miscible CO_2-WAG injection [7]. Though there have been attempts to calculate relative permeabilities on theoretical grounds, by far, the most common source of k_r curves has been experimental measurements [6]. Therefore, coreflood experiments have to be designed efficiently to provide relevant information about the complex two and three-phase flow mechanism. The

* Corresponding author: jorgeatovar@hotmail.com

experimental measurements must be accurate and representative of the system as they are key reservoir parameters such as trapped gas saturation, relative permeability curves and hysteresis effects [7].

Some studies present a valuable data set for the evaluation and simulation of CO_2 injection [8, 9]. These works carried out in carbonates and other rocks from oil reservoirs at in situ conditions, showed interesting results such as a relation between residual saturations and heterogeneity of the rock. They also showed a most favorable mobility ratio when brine displaced CO_2 and observed a change in the pore structure of carbonate rocks due to mineral reactions (dissolution and precipitation) that possibly affects the relative permeability displacement behavior of CO_2 and brine.

This work proposes an experimental study of unsteady-state relative permeability curves carried out in a Brazilian Pre-Salt reservoir rock sample at reservoir conditions (8500 psi and 70°C). The study involved both drainage and imbibition tests using equilibrated carbonated brine and $scCO_2$. In Situ Saturation Monitoring (ISSM) by CT and mass balance were used to trace the saturation evolution during the displacements. Finally, relative permeability curves were determined using the Corey model [10], and the Land trapping coefficient [11] was calculated along the length of the rock sample. Also, a robust experimental setup was commissioned for two- phase unsteady-state relative permeability curves testing.

2 Materials

2.1 Core samples

The reservoir carbonate rock samples were obtained from the oil zone of a Brazilian Pre-salt province field located in the Santos Basin, and its likely oil wet preference has been proven by the operator. In the experiment, a composite core of five short cores was used. An X-ray image of the composite core is showed in Figure 1. The composite core was arranged according to the dolomite content of each sample. Thus, the core samples were ordered from higher to lower dolomite content from injection to production; aiming to preserve the condition of the samples throughout the tests using CO_2 and carbonated brine. The average mineral content and the petrophysical measurements of the composite core are shown in Tables 1 and 2, respectively. The mineral composition of the rocks was provided by the company that provided the samples. Absolute gas permeability and effective porosity were measured using a gas permeameter (CoreLab Ultraperm-500) and a gas porosimeter (CoreLab Ultrapore-300), respectively. Figure 2 shows the initial porosity distribution profile obtained from N_2 and deionized water CT scans. A high degree of heterogeneity in porosity is noted since values obtained vary from 0.09 to 0.24. It should be noted that before the measurements, the samples were cleaned by Soxhlet extraction using toluene and methanol as recommended by Torsaæter and Abtahi [12]. Even though the wettability of the cores may be turned back to strong water wet preference, this process was needed since the use of the porosimeter and permeameter from initial measurements requires the samples in dry conditions.

Figure 1. X-ray image of the composite core.

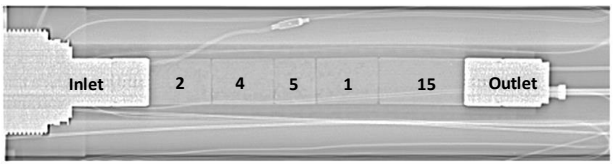

Figure 2. Initial porosity distribution profile

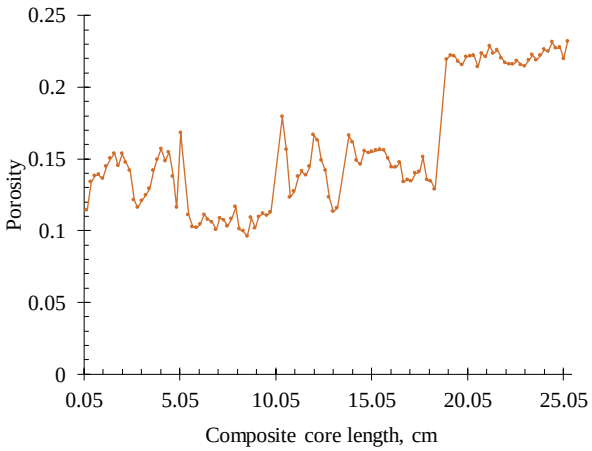

Table 1. Mineral content of the composite core.

Clay, %	Calcite, %	Dolomite, %	Others, %
2.72	57.19	31.94	8.15

Table 2. Petrophysics measurements of the composite core.

Length, cm	Diameter, cm	Permeability, mD	Porosity, %	Pore Volume, cm^3
25.28	3.78	182	15.72	44.71

2.2 Fluids

Two distinct fluids were used during the experimental work: supercritical CO_2 and equilibrated carbonated brine, both at reservoir conditions (8500 psi and 70°C).

2.2.1 Supercritical CO_2

Under laboratory conditions, CO_2 is found as a gas. Using a high-pressure compressor, CO_2 is transferred to the accumulators used in the test and pressurized until 4000 psi. Then, assisted by a positive displacement pump, the

fluid is raised to reservoir pressure. Table 3 presents some properties of CO_2 at reservoir conditions.

Table 3. CO_2 properties at reservoir conditions [13]

Pressure, psi	8500
Temperature, °C	70
Density, g/cm³	0.936
Viscosity, cp	0.103
Z factor	0.966

2.2.2 Equilibrated Carbonated Brine

Using a geochemical software, the injection of carbonated water in the carbonate rock saturated with seawater at reservoir conditions was simulated. The result of the simulation leads to the composition of the equilibrated carbonated brine. The objective of equilibrating the carbonated brine aimed two objectives: firstly, to avoid the mass transfer between the CO_2 and the carbonated brine while executing the test. Secondly, to control severe dissolution effects on the carbonate composite core. The ECB was prepared and fully saturated with CO_2 following a methodology proposed by Nuñez *et al.* [14]. Table 4 shows the equilibrated brine composition that was saturated with 45 cm^3 of CO_2 at lab conditions, then heated throughout a band heater until 70°C and pressurized using a positive displacement pump until 8500 psi. The viscosity of the ECB at reservoir conditions is 0.58 cp, as established by Rocha *et al.* [15].

Table 4. Equilibrated brine composition

Compound	Concentration, g/L
KCl	0.9490
$MgCl_2.6H_2O$	16.9717
$SrCl_2.6H_2O$	0.0272
$CaCl.2H_2O$	7.3213
NaCl	18.5128
Na_2SO_4	0.0587
$NaHCO_3$	9.0083
Na_2CO_3	0.0029
TDS	42.0230

2.3 Experimental setup

A robust experimental setup was designed and commissioned to perform unsteady-state relative permeability tests. The whole experimental setup was installed on and around a medical CT scanner Siemens Somatom Spirit (Figure 3).

Figure 3. Experimental setup

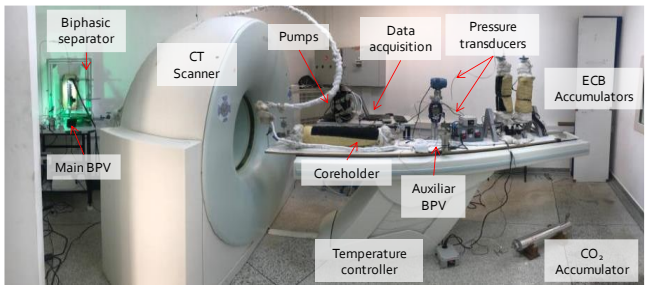

The experimental setup was divided into four major systems:

1) Injection system: composed of three Quizix Q5000 precision metering pumps used to displace fluids at a continuous flow rate and to execute the overburden pressure (1000 psi above the working pressure). Also, accumulators for fluids storage and injection.
2) Core sample confining system: composed by a special coreholder for relative permeability tests. The coreholder is made of aluminum designed for X-ray tomography. It includes a mixer that is a device made to avoid the gravity segregation effect while displacing fluids. Previous to the placing of the composite core into the coreholder, the samples were individually cemented (to fill surface irregularities) and stacked. Then, the composite core was wrapped with Teflon tape, aluminum foil, a heat shrinking film and then inserted into a nitrile rubber sleeve to avoid fluid leakage. Once the composite core was located inside the coreholder, a vacuum process of 24 hours was done to take out the air present in the porous medium. It was observed severe swelling effects in the Viton O-rings located both in the coreholder and accumulators that is why nitrile O-rings were used for the test. Also, there was presence of corrosion in the Teflon made packing seals of valves.
3) Production system: composed by a biphasic visual separator that allowed monitoring the produced fluid volume during the test at reservoir conditions (high pressure and high temperature). Also, a set of 2 (one principal and the other one auxiliary) back pressure valves (BPV) to ensure the execution of the test at 8500 psi.
4) Control and monitoring system: composed by differential and absolute pressure transducers, temperature controllers, a camera installed in the biphasic separator, and a laptop for data recording.

All the setup equipment (coreholder, accumulators, biphasic separator, and lines) were coated with band

heaters connected to temperature controllers to keep test temperature constant at 70°C.

3. Experimental procedures

3.1 Attenuation coefficient characterization

Once the fluids needed for the test were prepared, each attenuation coefficient (CT number) was determined. This procedure was executed by scanning with X-ray tomography, a hollow aluminum cylinder (Figure 4) filled with the fluid to study; the cylinder was located inside a coreholder at desired temperature and pressure conditions. The results of the attenuation coefficient with the temperature and pressure conditions are shown in Table 5.

Consecutively, the composite core was sequentially saturated with each fluid and brought to the conditions of Table 5. Then, CT scans were made along the saturated composite core to characterize the attenuation coefficient of 2 mm spaced slices. The CT values of the fluids and saturated composite were performed to obtain the parameters needed for in situ saturation calculation. The procedure is further explained in item 4.1.

Figure 4. Cylinder for fluids attenuation characterization

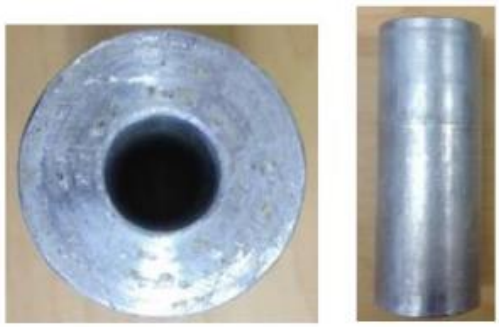

Table 5. Attenuation coefficients of fluids

Fluid	Temperature, °C	Pressure, psi	CT Number, HU
Nitrogen	70	500	-739
$scCO_2$	70	8500	31
Deionized water	70	8500	174
ECB	70	8500	200

3.2 Drainage test

Firstly, as the composite core was saturated with ECB at reservoir conditions (8500 psi and 70°C), the absolute permeability was determined while flowing it by changing the flow rate from 1 to 3cm^3/min and monitoring the pressure drop until equilibrium was reached. This absolute permeability, k, was established as the base permeability for further calculations of relative permeability.

The drainage was performed by displacing the ECB from the porous medium by injecting $scCO_2$ under reservoir conditions at a constant flow rate of 1 cm^3/min. This rate was chosen after reviewing the work of Vidal Vargas *et al*. [16], considering that lower rates would stimulate dissolution effects by increasing contact time, and higher rates could lead to damages inside the porous medium. The pressure drop and the produced ECB volume were monitored during the whole test. Also, CT scans were acquired for in situ saturation monitoring. CT scan parameters used were 130 kV and 80 mA. It is important to say that during the execution of the drainage test, an oscillation in pressure drop occurred caused by the severe volume expansion of $scCO_2$ when it decompressed rapidly from high (8500 psi) to atmospheric pressure, which ended up freezing and blocking the BPV for some seconds.

At the end of the drainage, the flow rate was increased to 1.5 cm^3/min in order to reach the residual ECB saturation. Then, as no more ECB was produced, the flow rate was pushed back to 1 cm^3/min until equilibrium was reached, and the effective permeability of $scCO_2$, k_{CO_2}, at residual ECB saturation was determined.

3.3 Imbibition test

Once the drainage was finished, the biphasic separator was adjusted to measure produced $scCO_2$. The imbibition was executed at reservoir conditions by injecting ECB at a flow rate of 1 cm^3/min. The criterion to choose the rate was the same used in the drainage test. During this process, the $scCO_2$ present in the porous medium at the end of the drainage was displaced up to residual or trapped $scCO_2$ saturation, $S_{CO_2 i}$. Before finishing the imbibition test, the flow rate was increased to 2 cm^3/min in order to reach the residual $scCO_2$ saturation, $S_{CO_2 r}$. Then, as no more $scCO_2$ was produced, the flow rate was decreased to 1 cm^3/min and, the effective ECB permeability, k_{ECB}, was determined.

At some time of the imbibition test (before 1 PV of ECB injected), the injection pressure exceeded the maximum allowable working pressure of the biphasic separator (10000 psi), most likely by the freezing effect in the BPV. Thus, the flow was re-addressed through the separator by-pass. Hence, the monitoring of produced CO_2 volume was lost, and it was only possible to keep tracing the saturation via CT scan.

At the end of the imbibition cycle, flow through cleaning injection was performed. It consisted in flooding the composite core with deionized water for 24 hours at reservoir conditions. Also, a CT scan of the fully deionized water saturated composite core was taken, in

order to obtain the required parameter for final porosity determination. However, the flow of deionized water could induce some changes in the porous medium. Then, the system was depressurized, and nitrogen flowed at 70°C and 500 psi. Concluding this stage, a final CT scan of the composite core saturated with nitrogen was taken. It was not possible to perform post-test porosity and permeability measurements due to the unavailability of the samples (they were required immediately for another research).

4. Results

4.1 Saturation evolution

As outlined above, the evolution of saturation was monitored by both mass balance and CT scan, except for the imbibition test, which was traced by CT scan only almost the whole test.

Equations (1) and (2) were used to determine the fluids saturation by mass balance for the drainage test.

$$S_1 = 1 - \frac{Vol_{1P}}{PV} \quad (1)$$

$$1 = S_1 + S_2 \quad (2)$$

Where,

S_1, Average displaced phase saturation
S_2, Average displacing phase saturation
Vol_{1P}, Produced volume of the displaced phase
PV, Pore volume

A MatLab™ routine, developed by Vargas [17], was used to process the CT scan images. The CT numbers obtained after that processing were then used in equations (3) and (4) to trace the saturation changes for each slice of the composite core during the experiment.

$$S_W = \frac{CT_R - CT_{NW}}{CT_W - CT_{NW}} \quad (3)$$

$$1 = S_W + S_{NW} \quad (4)$$

Where,

S_W, Wetting phase saturation
S_{NW}, Non wetting phase saturation
CT_R, Attenuation coefficient of the composite core saturated with biphasic saturation at a time of interest
CT_W, Attenuation coefficient of the composite core completely saturated with the wetting phase
CT_{NW}, Attenuation coefficient of the composite core completely saturated with the non-wetting phase.

4.1.1 Drainage test saturation evolution

Figure 5 shows the produced volume of ECB as a function of the injected volume of $scCO_2$. The curve displays an approximately linear behavior increase until 30 cm^3 of $scCO_2$ injected (red dot). The curve presents a change in its inclination caused by the beginning of biphasic flow at the end of the composite core. This turning point is the breakthrough [18]. From here, the produced volume of $scCO_2$ increases, and the produced volume of ECB gradually drops until a residual volume of ECB (higher than the ECB irreducible volume, as the plateau was not accomplished according to Figure 5) is achieved inside the sample.

Figure 5. Produced ECB

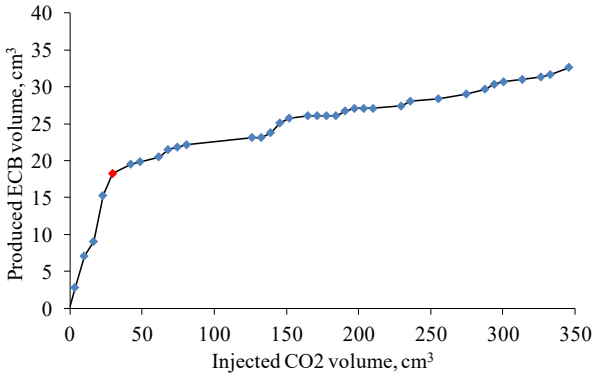

Figure 6 shows the evolution of $scCO_2$, and ECB average saturation (determined by mass balance) as a function of the pore volumes of $scCO_2$ injected during the drainage test. The graph depicts a rapid increase of $scCO_2$ saturation as a decrease in ECB saturation until approximately 0.6 PV of $scCO_2$ injected. Then, both curves perform an alteration on its inclination; this changing point represents the breakthrough as well. Also, on this Figure, it is possible to find that the breakthrough happened at an approximately ECB saturation of 0.6, and after almost 8 PV of CO_2 injected, a residual ECB saturation of 0.27 was achieved, which indicates that the ECB irreducible saturation will be less than 0.27.

Figure 6. Saturation evolution by mass balance

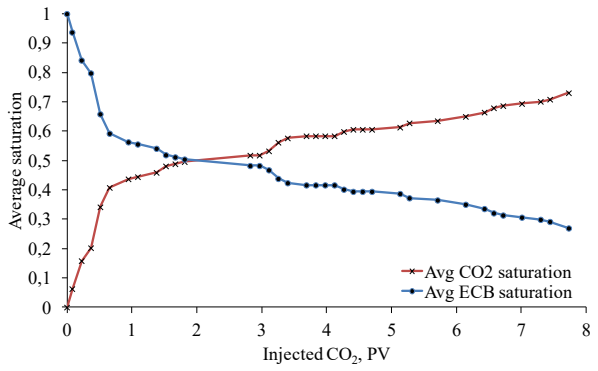

As part of the mass balance analysis, Figure 7, which is a zoom of the beginning of Figure 5, shows that the

volume of ECB produced from the beginning up to the breakthrough does not correspond to a linear behavior of 45° (depicted by the dashed line). This behavior, as explained by Rosa *et al*. [18], would correspond to an evidence of viscous fingering that occurred during the drainage test as a result of the unfavorable mobility ratio of $scCO_2$ displacing ECB (M = 5.01). As $scCO_2$ is more mobile than water in the porous medium, the injected $scCO_2$ tends to bypass water developing a less efficient displacement. Also, it could have been a consequence of having the composite core in a horizontal position, what could have promoted gravity segregation of fluids. The CT scanner used in this work is not adjusted for vertical scanning of the composite core, which would have been desirable in this case to minimize gravity segregation and viscous fingering. In addition, there could have been presence of mass transfer between the phases, since during the test the pressure of the system was occasionally higher that the equilibrium pressure of the two fluids (8500 psi). On the other hand, the compressibility of CO_2 at test conditions was determined (0.0001176 psi^{-1}) and could be negligible once there were not significant pressure changes.

Figure 7. Produced ECB during the first PV of CO_2 injected

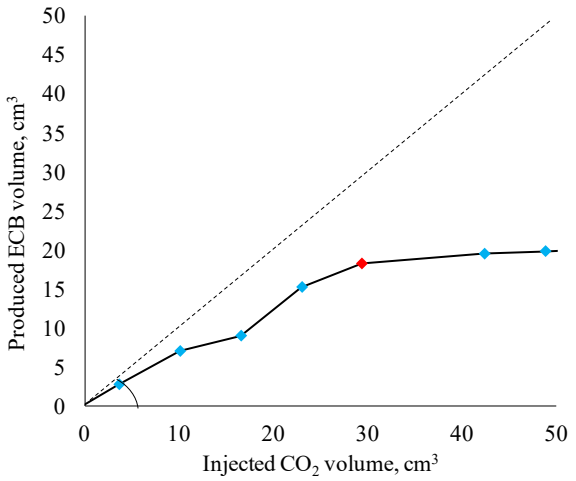

Figure 8 shows a comparison between the average $scCO_2$ saturations obtained by mass balance and computed tomography. On the chart, it is possible to see the proximity of saturation values from the measurements taken at an approximately same time (pore volumes of injected CO_2), e.g., the values of saturation taken at 1.6, 2.9, and 3.7 PV of $scCO_2$ injected among others. This proximity allows confirming the correspondence between the two saturation evolution monitoring methods used in this study, as well as the validation of the saturation values. However, there are some other values of saturations provided by CT that do not correspond to the ones of mass balance taken approximately at the same time, e.g., 0, 2, 6, and 8.2 PV of $scCO_2$ injected. One reason for such differences is the loss of capillary continuity between the core samples at each face to face junction. This, was verified by comparing one of the X-ray images of the composite core with the saturation distribution profiles obtained from each CT scan. This analogy allowed identifying that at every face to face joining position existed gaps that match with distortions of the saturation values tendency (even negative saturation values). The correlation between the two mentioned elements is presented in Figure 9. The upper part corresponds to the composite core X-ray image, and the gaps existing at each face to face junction are correlated to a saturation distortion on two saturation profiles downwards following the dashed lines. Also, errors associated to the measurement techniques and equipment might have contributed to the distortions in saturation. It is important to note that only saturation values between 0 and 1 were used to calculate the average saturation. Negative and values greater than 1 are presented in Figure 9 to depict the effect of loss of capillary continuity. On the other hand, the capillary end effect is less pronounced than the effects observed in water wet cores showed by Huang and Honarpour [19]. Hence, it might be assumed that the composite core of this study does not have a strong water preference, at least in the presence of $scCO_2$.

Figure 8. Saturation evolution by mass balance Vs computed tomography

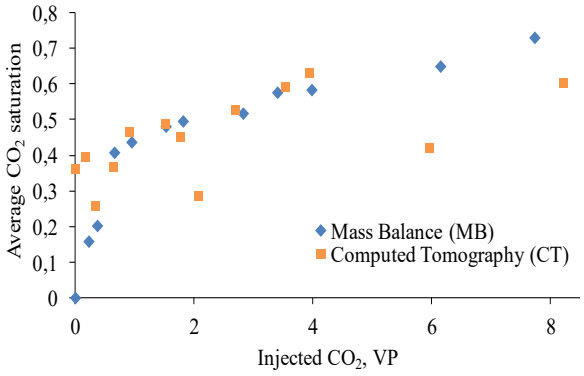

Figure 9. Correlation between composite core X ray image and drainage saturation profiles

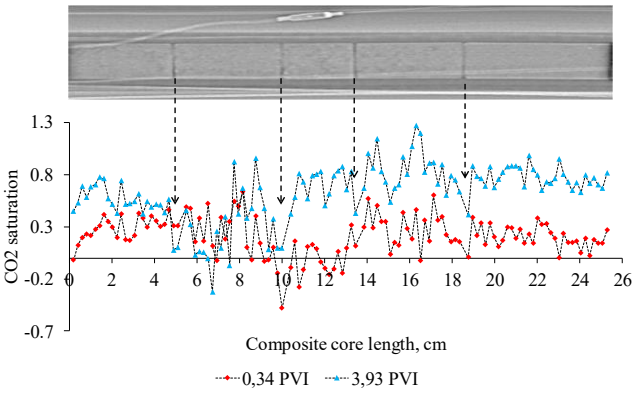

4.1.2 Imbibition test saturation evolution

As previously said, it was not possible to monitor the saturation evolution of the entire imbibition test by the mass balance due to the demand for bypassing the biphasic separator because of the pressure increase above

its working pressure. Hence, from that point, the saturation was traced by CT only.

Thus, to compose a complete imbibition saturation curve, the first values of ECB saturation obtained by mass balance were integrated with those taken from CT. Figure 10 presents the result of that integration. The saturation curve of the imbibition is represented by the black curve named "adjust", which starts at an average value of ECB saturation of 0.23 (residual value of ECB in the drainage). Thus, the curve continues through the saturation values obtained by mass balance until approximately 0.6 PV of ECB injected. From there, the values obtained by CT were used until the end of the imbibition, some values of saturation taken by CT (those close to 2 PV of ECB injected) were not taken into account for the curve, as they do not make physical sense in the saturation field.

Moreover, the adjusted curve presented a shifting point in the inclination at the approximate value of 0.8 PV of ECB injected. This point corresponds to the breakthrough of the ECB. In this case the displacement process occurred at a more favorable mobility ratio (M = 0.1), and as stated by Fanchi [20] the ECB displacing CO_2 is a more efficient displacement. Also, Figure 10 shows low post breakthrough $scCO_2$ recovery. This could imply that the sample is not strongly water wet in presence of $scCO_2$ which would be wetting the sample surfaces to certain extent and not behaving like a non-wetting gas.

Figure 10. Saturation evolution by mass balance plus computed tomography

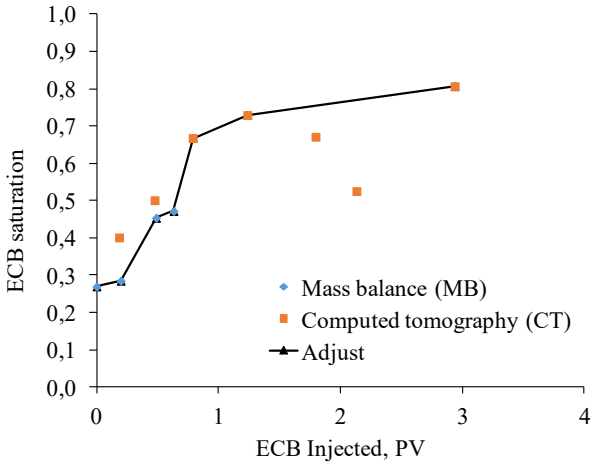

At the end of the imbibition, a trapped $scCO_2$ saturation value of approximately 0.195 was obtained, which means that a significant pore volume of the porous medium was able to be filled again with ECB (almost 0.8 of saturation).

Figure 11 shows the composite core X-ray image and two saturation distribution profiles obtained by CT scan at different times (0.19 and 0.48 PVI of ECB). In this chart, it is possible to correlate the gaps between each face to face junction of the core samples with the saturation profiles along the composite core. Here the saturation distributions profiles were also affected by the loss of capillary continuity, but less drastically than in the drainage test probably because of the improvement of the displacement efficiency or the water wet preference of the rock.

Figure 11. Correlation between composite core X ray image and imbibition saturation profiles

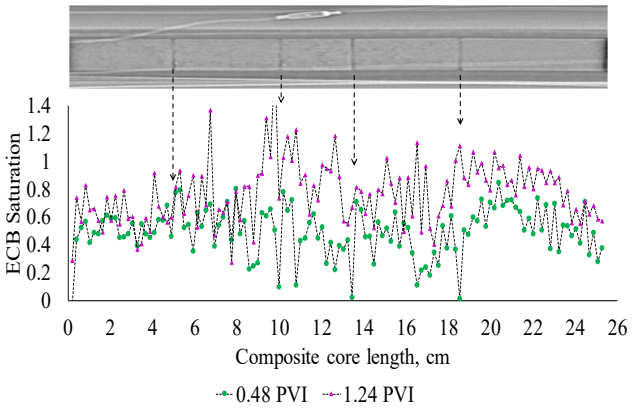

4.2 Relative permeability curves

At the beginning of the study, it had been planned to use the JBN method to determine the relative permeability curves. However, there were some experimental conditions such as unstable displacement (presence of viscous fingering) and not constant flow rate or pressure drop while executing the displacements; that disallowed the use of that methodology.

As previously said, no theoretical expression exists for the relative permeability function. However, when analytical expressions are needed, it is possible to use the following exponential form called Corey model [6]:

$$k_{r1} = k_{r1}^{o}\left(\frac{S_1 - S_{1r}}{1 - S_{1r} - S_{2r}}\right)^{n_1} \quad (5)$$

$$k_{r2} = k_{r2}^{o}\left(\frac{1 - S_1 - S_{2r}}{1 - S_{1r} - S_{2r}}\right)^{n_2} \quad (6)$$

Where,

k_{r1}, displacing phase relative permeability
k_{r2}, displaced phase relative permeability
k_{r1}^{o}, displacing phase relative permeability end point
k_{r2}^{o}, displaced phase relative permeability end point
S_1, saturation of the displacing phase
S_{1r}, connate saturation of the displacing phase
S_{2r}, residual saturation of the displaced phase
n_1, displacing phase Corey exponent
n_2, displaced phase Corey exponent

Table 6 shows a summary of the results of residual saturations and the relative permeability endpoints determined from the drainage and imbibition tests. The absolute permeability measured with ECB at the

beginning of the drainage test was taken as the base permeability, relative permeability endpoints were determined using Darcy's law, and the residual saturations were taken from the measurements of average saturation from mass balance and CT for drainage and imbibition respectively. Also, Table 7 presents the Corey exponents, n_1 and n_2, that were used in the model. These coefficients are not directly related to the mineralogy or properties of the rock used in this work. However, they were extracted from a research work realized in carbonates at reservoir conditions as well [9].

Table 6. Results summary

Stage	Pressure drop, atm	Permeability, mD	Relative permeability
ECB @ 100%	0.10	209.7	1
CO_2 @ S_{ECBr}, 27%	0.02	187.6	0.89
ECB @ S_{CO_2r}, 19.5%	0.21	99.3	0.47

Table 7. Corey exponents

Process	n_1	n_2
Drainage	1.91	4.14
Imbibition	2.92	2.74

Where,

n_1, displacing phase Corey exponent
n_2, displaced phase Corey exponent

Consequently, using the values of saturation obtained during the test and the data of Tables 6 and 7, equations (5) and (6) were applied to construct the drainage and imbibition relative permeability curves (Figure 12).

Figure 12. Relative permeability curves

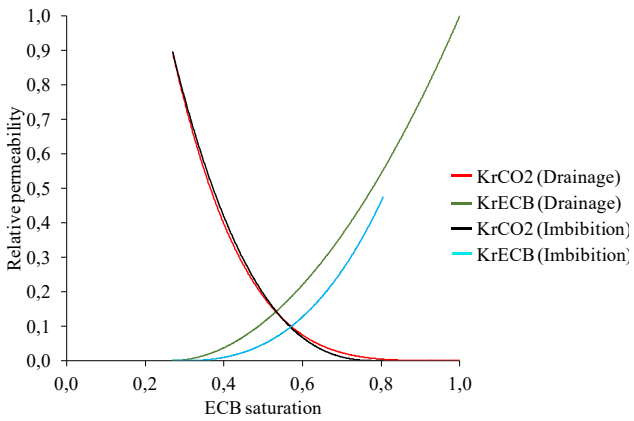

First of all, relative permeability is a rock fluid property that has a strong dependency on the saturation of the phases present in the porous medium. However, the relationship between relative permeabilities of these phases and their saturations are also a function of rock properties (pore size distribution, for example) and wettability [6,20]. As it is well known for gas-liquid systems, the wettability in this case would have a preference for the ECB. However, the value of S_{ECBi} reached at the end of the drainage (less than 0.27) could be an indication of weak wetting preference to ECB; since a rock with a stronger wetting preference would have reached a higher S_{ECBi}.

Also, it is vital to take into account that the cleaning process performed in the core samples may have not changed severely the wettability of the carbonate samples. In contrast to the results showed by Austad *et al*. [22].

Besides that, other features that can be observed in Figure 12 are the critical gas saturation, and the behavior of ECB and $scCO_2$ relative permeability curves. The critical gas saturation, that is, the value at which the nonwetting phase becomes mobile, is located at an approximate value of $scCO_2$ saturation of 0.20. According to Amyx *et al*. [21], this saturation value may vary between 0.10 and 0.30 of nonwetting saturation in carbonates. The relative permeability curves behavior could be some indicator of the distribution of the fluid within the porous medium [21]. There is a rapid decline in the ECB relative permeability for small increases in $scCO_2$ saturation, which would indicate that the larger pores or longer flow paths are occupied first by the $scCO_2$. Also, as little $scCO_2$ volume has been injected into the porous medium after the critical gas saturation, there is a rapid rise in $scCO_2$ relative permeability for small increases of this phase saturation, this would confirm that above the critical gas saturation, the average pore size saturated with the ECB becomes successively smaller, which means that the $scCO_2$ would occupy larger pores within the porous medium.

In addition, the trapped $scCO_2$ saturation at the end of the imbibition test achieved a value of 0.19, close to the average saturation of 0.23 reported by Bennion and Bachu [9]. This study and the one presented by Bennion and Bachu showed low values of porosity (0.15 and 0.12 respectively). This direct relationship between trapped gas saturation and porosity differs from the result obtained by Jerauld [23] in water wet samples, which shows higher values of gas trapped saturation for similar values of porosity. The divergence in porosity and trapped gas in this study may be an evidence that the ECB is not strongly wetting the sample and would indicate that the $scCO_2$ had certain wetting tendency that prevents it from being capillary trapped like a non-wetting fluid.

On the other hand, the hysteresis effect was confirmed in the relative permeability curve of the ECB. This effect could be associated with the $scCO_2$ trapping by the ECB within the porous medium during the imbibition process, which decreases the conductivity offered to the ECB.

However, the $scCO_2$ relative permeability curve does not present a significant change; this probably caused by the slippage effect of supercritical $scCO_2$. To better depict the hysteresis effect, the Land´s trapping parameter, *C*, was determined along the composite core by using Equation (7).

$$C = \frac{1}{S_{CO_2 i}} - \frac{1}{S_{CO_2 c}} \qquad (7)$$

Where,

C, Land trapping parameter
$S_{CO_2 i}$, Residual or trapped $scCO_2$ saturation (at the end of the imbibition process)
$S_{CO_2 c}$, Initial or connate $scCO_2$ saturation (at the beginning of the imbibition process)

Figure 13 shows the Land trapping parameter for each CT scan slice taken from the composite core. According to the Land formulation, the lower the parameter, the higher the trapped gas saturation. Then, in line with Figure 13, the last 6 cm of the porous medium shows a lower trapping saturation tendency, contrary to the observed in the beginning (first 5 cm) of the composite core, which shows a lower tendency in Land parameter. This behavior could be related to changes in porosity along the composite core, which allowed to store more $scCO_2$ on zones of higher pore volume.

Figure 13. Land trapping parameter

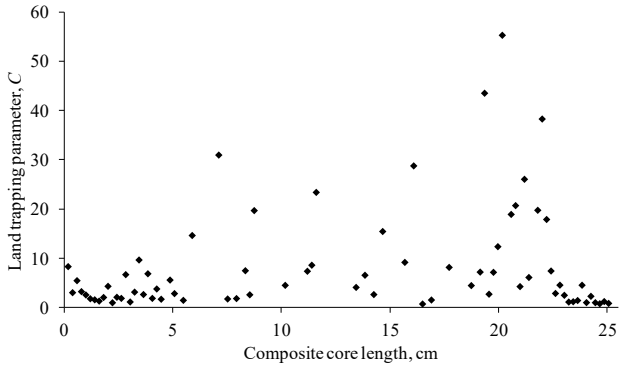

5. Conclusions

This work presents a novel literature example of relative permeability using $scCO_2$, given that was carried out at real reservoir conditions in Brazilian Pre-salt carbonate rock samples while similar studies are realized using outcrop rocks at laboratory conditions.

It was confirmed the presence of viscous fingering of $scCO_2$ using a produced volume graph analysis. The fingering effect was probably instigated by executing the test in horizontal position. It was observed a more favorable mobility ratio of the imbibition process than in the one of the drainage, caused by the increase of viscosity of the displacing phase. Also, the low post breakthrough $scCO_2$ recovery and the low trapped $scCO_2$ at the end of the imbibition might be an evidence that the ECB is not strongly wetting the samples in presence of $scCO_2$. In addition, the loss of capillary continuity could be evidenced by correlating an X-ray CT image of the composite core and saturation profile distributions, this phenomenon affected some saturation measurements. In addition, there could have been presence of mass transfer between the phases altering the produced volumes in the separator.

It is valid to say that the final saturation reached in each displacement corresponds to a residual saturation instead of an irreducible saturation.

As the JBN methodology was not possible to be applied in this work, Corey coefficients corresponding to rocks from other similar study were used. Hence, the shape of the relative permeability curves determined in this work, could not represent accurately the behavior of the relative permeability.

It could be drawn that despite the cleaning process of the carbonate core samples using toluene and methanol, the wettability of those rocks did not achieve an entirely turn from oil-wet to water-wet.

The hysteresis effect was evidenced on ECB relative permeability curve. However, the $scCO_2$ curve did not present a significant change. The Land trapping parameter was determined all along the composited core allowing detecting the potentials zones of $scCO_2$ trapping in the porous medium.

It is recommended not to use Viton O-rings for the coreholder and accumulators in order to avoid severe swelling of the seals. For better performance it is recommended to use nitrile O-rings. Also, it is strongly suggested to ensure the heating of the back-pressure valve located at the production outlet to avoid freezing by $scCO_2$ expansion. In addition, to avoid leaks trough valves, it is indicated to change its standard Teflon made packing seal for packing seals made of PEEK (Polyether Ether Ketone).

The authors acknowledge Repsol Sinopec Brazil S.A, and the Brazilian National Petroleum, Natural Gas and Biofuels Agency (ANP) for the financial support. Also, the University of Campinas (UNICAMP), the Center for Petroleum Studies (CEPETRO) and the Laboratory of Miscible Methods of Recovery (LMMR) for intellectual and technical support.

6. References

1. E. de Almeida, L. Colomer, W. Vitto, L. Nunes, F. Botelho, F. Costa, L. Waeger. *Gás do Pré-sal: oportunidades, desafios e perspectivas* (IBP – UFRJ, Rio de Janeiro, 2017)
2. Agencia Nacional de Petróleo, Gás e Biocombustíveis. Resolução N° 806, de 17 de Janeiro de 2020 (Diario oficial da união, seção 1, ISSN 1677-7042, 2020)

3. H. Rodriguez, E. Mackay, D. Arnold, D. Silva. Optimization of CO_2-WAG and calcite scale management in pre-salt carbonate reservoirs. Offshore technology conference, Brazil (2019)
4. B. Caudle, A. Dyes. Petroleum Transactions, AIME. **v** 213, p. 281-283 (1958)
5. P. Laboissière, R. Santos, O. Trevisan. Carbonate pretrophysical properties: computed tomography (CT) for experimental WAG design under reservoir conditions. Offshore technology conference, Brazil (2013)
6. L. Lake. *Enhanced oil recovery* (Prentice Hall, ISBN 0-13-281601-6, New Jersey, 1989)
7. S. Duchene, G. Puyou, P. Cordelier, J. Hy-Billiot, G. Hamon. Efficient experimental data adquisition for miscible CO_2-WAG injection corefloods in carbonate. SPE improved oil recovery symposium, Tulsa, 2014
8. B. Bennion, S. Bachu. SPE Reservoir evaluation engineering J. i. **June**, p. 487-496 (2008)
9. B. Bennion, S Bachu. Drainage and imbibition CO_2/brine relative permeability curves at reservoir conditions for carbonate formations. SPE ATCE, Florence (2010)
10. A. T. Corey. Prod. Monthly. 19 (1), 38. Nov (1954)
11. C. Land. AIME Transactions. **v.** 243, p. 149-156 (1968)
12. O. Torsæter, M. Abtahi. *Experimental reservoir engineering laboratory work book* (NTNU, Trondheim, 2000)
13. Peace software. Calculation of thermodynamic state variables of carbon dioxide. 2019. Access in: <https://www.peacesoftware.de/einigewerte/co2_e.html>
14. R. Nuñez, R. Vaz, E. Koroishi, J. Vargas, O. Vidal. Investigation of dissolution effects on dolomite porous media under carbonated water injection CWI. SPE Abu Dhabi international petroleum exhibition and conference, Abu Dhabi (2017)
15. E. Rocha, O. Vidal, E. Koroishi, J. Vargas, L. de Oliveira. Materials science fórum. **v**. 965, p. 69-77 (2019)
16. J. A. Vidal Vargas, E. Y. Yasuda, E. T. Koroishi. O. V. Trevisan. Applied Geochemistry 113 (2020) 104502
17. J. Vargas. *Determinação dos parâmetros de convecção- dispersão- transferência de massa em meio poroso usando tomografia computadorizada* (PhD. Thesis, Universidade Estadual de Campinas, Brazil, 2015)
18. A. Rosa, R. Carvalho, J. Xavier. *Engenharia de reservatórios de petróleo* (E Interciência ltda, Rio de Janeiro, 2006)
19. D. Huang, M. Honarpour. Journal of Petroleum Science and Engineering. 19 (1998) 103-117
20. J. Fanchi. *Integrated reservoir asset management* (E Gulf Professional Publishing, Burlington, 2010)
21. J. Amyx, D. Bass, R. Whiting. *Petroleum reservoir engineering* (E McGraw Hill Inc, New York, 1988)
22. T. Austad, S. Strand, T Puntervold, R. Ravari. New method to clean carbonate reservoir cores by seawater. International symposium of the society of core analysts, Abu Dhabi, 2008
23. G. Jerauld. SPE Reservoir Engineering, 12(01), p. 66-73 (1997)